Am J Transl Res 2019;11(6):3761-3770
www.ajtr.org /ISSN:1943-8141/AJTR0090864

Original Article

Factors impacting technical success rate of image-guided intra-arterial therapy in rat orthotopic liver tumor model

Hideyuki Nishiofuku[1], Andrea C Cortes[2], Joe E Ensor[3], Adeeb A Minhaj[2], Urszula Polak[2], Mirtha S Lopez[2], Ryan Kiefer[4], Stephen J Hunt[4], Kimihiko Kichikawa[1], Marshall E Hicks[2], Terence P Gade[4], Rony Avritscher[2]

[1]Department of Radiology, Nara Medical University, 840 Shijo-cho, Kashihara 634-8522, Japan; [2]Department of Interventional Radiology, The University of Texas MD Anderson Cancer Center, Houston 77030, Texas, USA; [3]Houston Methodist Cancer Center, Houston Methodist Research Institute, Houston 77030, Texas, USA; [4]Department of Radiology, Hospital of The University of Pennsylvania, Philadelphia 19104, Pennsylvania, USA

Received January 4, 2019; Accepted April 20, 2019; Epub June 15, 2019; Published June 30, 2019

Abstract: Transcatheter hepatic arterial chemoembolization (TACE) is the current standard of care for intermediate stage hepatocellular carcinoma (HCC) patients. To study the effects of TACE in the tumor immune microenvironment, an immunocompetent rat model is required. The purpose of this study was to determine factors influencing technical success during hepatic arterial catheterization in immunocompetent orthotopic rat liver models. To this end, 91 Sprague-Dawley and eighty-three F344 rats underwent transcatheter hepatic arterial embolization using a transcarotid approach and were divided into a non-tumor-bearing (n = 41) and tumor-bearing (n = 133) groups. Vascular diameters of the hepatic arterial branches were evaluated from angiographic images. Catheterization of the proper hepatic artery (PHA) was achieved in 92% of the tumor-bearing and 68.3% of the non-tumor-bearing rats. We found a strong positive association between the diameter of the PHA and animals' body weight in both groups ($P < 0.005$), independently of the rat's strain. Results of the logistic regression model predicting a successful catheter placement into the PHA according to the animal's weight indicate that successful PHA catheterization is likely to be achieved in tumor-bearing animals weighing ≥ 250 g and > 308 g in non-tumor-bearing rats, with a sensitivity and specificity of 91.3% and 100.0% and 96.4% and 92.3%, respectively. In conclusion, animal's body weight at the time of catheterization is the principal determinant of technical success for transcatheter arterial embolization. Familiarity with these technical factors during animal selection will improve TACE technical success rates.

Keywords: Transcatheter arterial embolization, hepatocellular carcinoma, technical success, body weight, arterial access and endovascular treatment

Introduction

Transcatheter hepatic arterial chemoembolization (TACE) is the current standard of care for intermediate stage hepatocellular carcinoma (HCC) patients. TACE has shown improved survival rates and is an integral part of the Barcelona Clinic Liver Cancer guidelines [1]. In advanced HCC, systemic therapies are well-established with molecular targeted therapies, such as sorafenib and lenvatinib approved for first-line therapy [2] and now also nivolumab, a PD-1 immune checkpoint inhibitor antibody [3], as the second line of treatment. Despite these important clinical advances, treatment outcomes remain poor.

Optimal combination therapy using image-guided intervention and molecularly targeted agents could offer synergistic effects in HCC therapy and improve outcomes. Investigational efforts to address this unmet need requires robust preclinical research platforms and relevant animal models for interventional oncology (IO) research. Animal models for IO must exhibit sufficient anatomic size to mimic treatment protocols using doses and devices easily translated into clinical practice. Traditionally, large animals such as pigs, dogs, and rabbits have been considered more appropriate research subjects for complex endovascular experimentation and noninvasive imaging development, due simply to ease in vascular access and catheterization.

Unfortunately, there is a dearth of molecular biology tools available for these large animal models.

The laboratory rat (Rattus norvegicus) has recently gained popularity in IO research. These animals offer ample access to advanced molecular biology tools, and their biological processes can be fully characterized, unlike their large animal counterparts [4, 5]. Particularly relevant is the fact that in the era of fundamental immunotherapy advances, immunocompetent syngeneic rat liver tumor models are available for IO research [6]. In order to successfully use rat models, the investigator must be familiar with the rat vascular anatomy and advanced endovascular techniques. The majority of the literature applying rat models in IO research reported the use of gastroduodenal artery (GDA) as a route to access the hepatic arterial vasculature [7-11]. This approach requires proximal and distal ligation of the GDA artery at the end of the procedure [12-14], impacting the blood supply to the digestive system and often requiring protracted exposure of abdominal viscera during surgical instrumentation. Another common method uses a selective hepatic artery catheterization via left common carotid approach under direct visualization [15, 16]. This procedure reduces ischemia to the digestive system, but requires a simultaneous laparotomy and a direct visualization of the catheter guidance to accurately place the catheter tip into the hepatic artery. A novel technique that obviates the need for a concomitant laparotomy has been described using transfemoral [16, 17] or transcarotid approaches [16, 18] with fluoroscopy-guided hepatic arterial catheterization. This approach dramatically reduces procedural time and surgical trauma, presumably diminishing the expression of inflammatory cytokines and minimizing the extent of tissue remodeling that can interfere with immunology research. This sophisticated procedure requires advanced knowledge of key technical considerations unique to rat anatomy, in order to ensure successful hepatic catheterization. The present study aims to establish the determining factors that influence technical success during transcatheter arterial embolization using a transcarotid approach in rat liver tumor models for preclinical research in interventional oncology.

Materials and methods

Animal models

All studies were approved by our institutional animal care and use committee and were performed in accordance with institutional guidelines. Animals were housed under standard temperature and light-dark schedule (12 h light-dark cycles), in a pathogen-free environment, and were allowed free access to rodent chow and water. For all surgical procedures, animals were anesthetized using 2-3% isoflurane and monitored for the depth of anesthesia throughout the procedures. Aseptic surgical techniques were used, and adequate steps were taken routinely to ensure animal comfort during recovery.

Tumor-bearing animals (n = 133) were inoculated with 5×10^6 N1S1 Novikoff hepatoma cells (ATCC, Manassas, VA, USA) syngeneic to Sprague-Dawley rats (Charles River Laboratories, Wilmington, MA, USA) or 1×10^7 RCN-9 cells (RIKEN BioResource Research Center, Tsukuba, Japan) syngeneic to F344 (CLEA Japan, Tokyo, Japan) rats. Cell suspensions (100 μL) were injected by using a 25-gauge needle into the subcapsular portion of the left hepatic lobe after performing a midline laparotomy. Immediately after the cell injection, a small square of BloodSTOP (Mountain View, CA, USA) was used on the site of injection to achieve hemostasis and prevent cell reflux. Tumor nodules were allowed to grow for seven days or 4 weeks for Sprague-Dawley and F344 rats, respectively.

Image-guided intra-arterial therapy

Ninety-one adult male Sprague-Dawley (SD) rats and eighty-three F344 rats underwent hepatic arterial catheterization using a transcarotid approach and were divided into a non-tumor bearing (n = 41) and tumor-bearing (n = 133) groups. Animal hair clippers were used to shave the ventral neck region from the chin to the sternum. Vascular access of the left common carotid artery was achieved by a superficial straight incision, slightly to the right of the midline of the neck to the top of the sternum. Subsequently, skin on both sides of the incision was separated, and a blunt-dissection was made to expose the muscular layer (**Figure 1A**, **1B**). Curved, smooth, sharp hemostat forceps

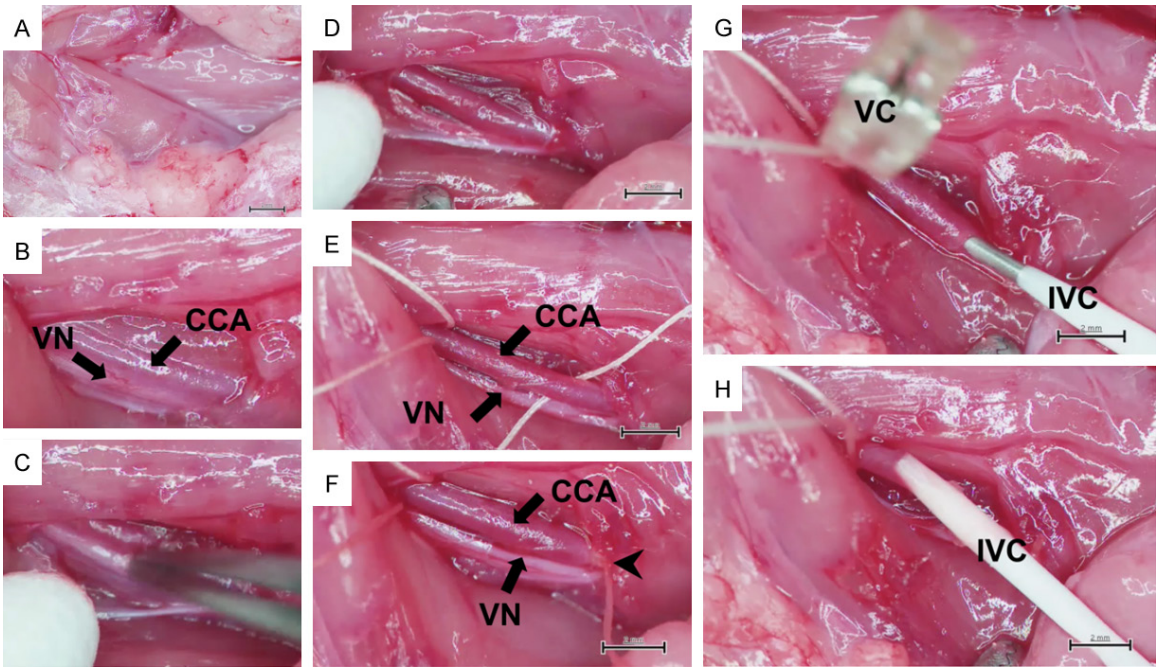

Figure 1. Pictorial description of the critical steps involved in the common carotid artery cannulation. A. Shows the externalization of the muscular layer after a superficial incision from the midline of the neck to the top of the sternum. B. Left common carotid artery (CCA, black arrow) and vagus nerve (VN, white, black arrow) within the CCA sheath. C, D. Photographs showing the dissociation of the vagus nerve from the adjacent common carotid artery. E. Ideal anatomical placement of the vascular loops (4-0 silk suture) around the artery. F. Shows a double-knot surgical tie of the distal suture to the clip used as a retraction point prior to arteriotomy (arrowhead) and a second untied suture around the proximal portion of the CCA used for the arterial ligation immediately after the vascular catheter was withdrawn at the end of the procedure. G. Vascular clip (VC) placement to prevent retrograde blood flow followed by the insertion of the intravenous vascular catheter (IVC) into the arterial lumen. H. Advancement of the intravenous vascular catheter (IVC) through the vessel after the release of the vascular clip and needle retraction to avoid vessel damage. Scale bars represent 2 mm.

along with toothless microsurgical forceps were used to separate the remaining fat and muscle as well as the overlying fascia. The left common carotid artery (CCA) was further exposed by a continued blunt-dissection (**Figure 1C**, **1D**). The vagus nerve was carefully dissociated from the adjacent CCA, and a 4-0 silk suture was situated underneath the artery at the cranial and caudal ends of the exposed vessel (**Figure 1E**). A tight double knot was made in the distal portion of the CCA to block retrograde blood-flow and to gently tighten and pull the vessel out for catheterization (**Figure 1F**). A small vascular clip was placed at the proximal site of the incision to control the blow-flow (**Figure 1G**) and, immediately after, the CCA was cannulated (**Figure 1H**) by a 20-gauge intravenous catheter (Angiocath - IV catheter; 20G × 1.16) using a dissecting microscope. Custom made 40 cm long micro-catheters (Tokai Medical, Japan), 1.6-Fr for SD rats and 1.9-Fr for F344 rats and, a 0.014-inch guidewire (Transcend; Boston Scientific, USA) were inserted through the intravenous catheter into the arterial lumen. The microcatheter was subsequently advanced into the proper hepatic artery. Manual injection of iodixanol injectable contrast medium (Visipaque; GE Healthcare, USA), was delivered through the catheter, as needed, to visualize the hepatic vasculature. A final digital subtraction angiography (DSA) was performed to corroborate the final appearance of blood vessels (**Figure 2**). After the intervention, the intravenous catheter was removed, CCA was ligated, and the neck incision was closed by an uninterrupted suture and animal wound clips. A one-time injection of the analgesic buprenorphine (0.1-0.5 mg/kg) was administered immediately after surgery. Intra-arterial catheterizations were performed under fluoroscopic guidance by an experienced board-certified interventional radiologist. Technical success of the procedure was defined as the stable placement of the microcatheter tip into the proper hepatic

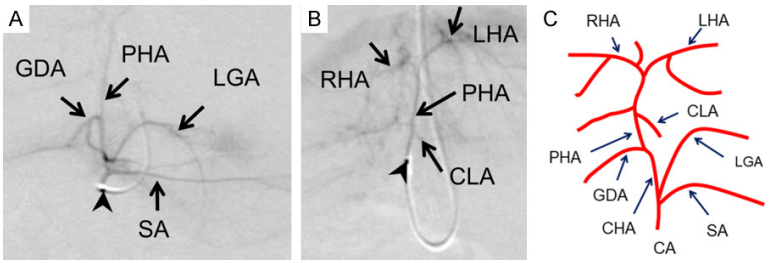

Figure 2. X-ray-based conventional digital subtraction angiography (DSA) delineating the normal arterial anatomy of Sprague-Dawley rats. Animals' vasculature is visible as darkened areas over a light grey background after the delivery of iodixanol injectable contrast medium through the catheter. A. DSA showing the normal anatomy of the proper hepatic artery (PHA), left gastric artery (LGA), gastroduodenal artery (GDA) and splenic artery (SA). B. Hepatic vascular angiography showing the proper hepatic artery (PHA) branching into the right (RHA) and left (LHA) branches and the location of caudal lobe artery (CLA). C. Simplified schematic illustration of the rat's celiac axis anatomy pertinent to hepatic artery catheterization. Arrowhead: microcatheter tip.

artery. The diameter of the proper (PHA), left (LHA) and right hepatic (RHA) arteries were evaluated from angiographic images, and each image was spatially calibrated by using the catheter tip as a reference. For further anatomical reference, we have included representative images of our rats' angiograms (**Figure 2A**, **2B**) and a schematic diagram of the SD rat's celiac axis (**Figure 2C**). Imaging analyses were carried out using Fiji image processing package [19]. Animal weight was recorded at the time of angiography.

Statistical analysis

The normality of continuous variables was analyzed by using the Shapiro-Wilk tests. Wilcoxon rank-sum test was used to compare the differences in weight between groups. Spearman's rank correlation coefficient was used to evaluate the strength of association between animals' weight and the diameter of the PHA. A paired t-test was used to assess the differences between the diameter of RHA and LHA, and the Pearson product-moment correlation coefficient to measure the strength of linear association between vessel diameters. Subsequently, separate linear regression models were developed to identify the interaction between the presence of tumor or rats' strain on the relationship between body weight and PHA diameter, using the diameter of the PHA as the response variable. Finally, a logistic regression model was fitted to the non-tumor or tumor-bearing SD rats using the success of the procedure as the response variable and animals' weight as the predictive factor. The fit of the logistic regression model was evaluated by the area under the receiver operating characteristic curve (AUC), and the sensitivity and specificity of the selected cut points were assessed. Results were expressed as median [range] or mean ± (Standard Deviation [SD]) of non-normally and normally distributed data, respectively. All analyses were carried out using SAS 9.4. A value of $P < 0.05$ was considered significant.

Results

Overall median body weight and range of the three cohorts combined was 295 g [227-477]. Tumor-bearing rats (n = 133) at the time of catheterization exhibited a median weight and range of 285 g [227-477], and non-tumor bearing rats (n = 41) had a median weight of 331.2 g [236.6-437]. There were no significant differences in body weight between tumor-bearing rats of different strains, with a median weight of 299 g [227-477] and 282 g [240-475] for SD and F344 rats respectively ($P = 0.80$). Similarly, the body weight of tumor-bearing rats compared to those without tumor from the same strain was not significantly different ($P = 0.19$).

Correlation between body weight and diameter of the proper hepatic artery

The results of the present study revealed that there is a strong positive correlation between the body weight and diameter of the PHA ($P < 0.005$). More importantly, the dependence between these factors was observed among the groups, with F344 rats demonstrating the strongest degree of association, with a Spearman's rank correlation coefficient and 95% confidence interval of 0.87 [95% CI 0.80-0.91]; $P < 0.0001$. Non-tumor-bearing SD rats demonstrated the second strongest association with a positive correlation of 0.65 [95% CI 0.43-0.80]; $P < 0.0001$. Finally, tumor-bearing SD rats exhibited a positive correlation of 0.40 [95% CI 0.14-0.61]; $P = 0.004$.

Table 1. Significant differences between the diameter of the left and right hepatic artery branches in the three rat cohorts

Vessel	Mean (95% CI)	SD	*P*-value†
Sprague-Dawley Non-Tumor-Bearing Rats (n = 41)			
Body Weight 331 g [237-437]††			
PHA	0.57 mm (0.53-0.62)	0.14	
RHA	0.36 mm (0.33-0.39)	0.10	*P < 0.0001*
LHA	0.41 mm (0.37-0.44)	0.11	
Sprague-Dawley Tumor-Bearing Rats (n = 50)			
Body Weight 299 g [227-477]††			
PHA	0.59 mm (0.57-0.61)	0.07	
RHA	0.35 mm (0.32-0.38)	0.1	*P* = 0.0001
LHA	0.40 mm (0.38-0.42)	0.07	
F344 Tumor-Bearing Rats (n = 83)			
Body Weight 282 g [240-475]††			
PHA	0.50 mm (0.48-0.52)	0.07	
RHA	0.26 mm (0.24-0.27)	0.06	*P* < 0.0001
LHA	0.31 mm (0.30-0.32)	0.05	

PHA: Proper Hepatic artery, RHA: Right Hepatic Artery, and LHA: Left Hepatic Artery, mm: millimeter (s), g: grams, 95% CI: 95% Confidence Intervals of the mean value, SD: Standard Deviation. †Paired t-test, ††Body Weight: Median [minimum-maximum].

Table 2. Logistic regression model to predict the likelihood of technical success of the procedure based on animals' weight

Parameter	DF	Estimate	SE	Wald X^2	*P*-value
Sprague-Dawley Non-Tumor-Bearing Rats					
Intercept	1	56.63	29.91	3.59	0.058
Weight	1	-0.18	0.10	3.62	0.057
Sprague-Dawley Tumor-Bearing Rats					
Intercept	1	-27.85	16.08	3.00	0.083

DF: Degrees of freedom, SE: Standard Error, Wald X^2: Wald Chi-Square.

Differences between hepatic artery branches diameter

We found a significant difference in the mean diameter of the left hepatic artery compared with the diameter of the right hepatic artery (*P* < 0.0001). The size of the RHA was significantly smaller than the LHA in both rats' strains. The LHA remained constantly larger in the presence or absence of liver tumor. The specific dimensions of the hepatic artery vasculature are reported in **Table 1**. Additionally, we found a strong positive correlation between vessel diameters with Pearson's correlation coefficient r and 95% CI of 0.65 (0.56-0.73) for the relationship between PHA and RHA, 0.67 (0.58-0.74) and 0.71 (0.63-0.78) for PHA and LHA and RHA and LHA, respectively; P < 0.001.

Linear relationship between the diameter of the proper hepatic artery and the animals' body weight

Results of linear regression modelling further confirmed a significant positive linear relationship between the diameter of the proper hepatic artery and the animals' body weight. Interestingly, the results of the two separated linear regression models, in which we tested for interactions between the size of the PHA and body weight, in relation to (i) the presence of the tumor and (ii) rats' strain indicate that the relationship between weight and PHA diameter differs significantly between tumor-bearing and non-tumor bearing rats (interaction = -0.00114; *P* = 0.0004). We found that body weight (coefficient = 0.00147; *P* < 0.0001), and presence of tumor (coefficient = 0.40204; *P* = 0.0002) were significant predictors. However, a negative interaction term indicates that the diameter of the PHA does not increase as rapidly as the weight among tumor-bearing rats. Proper hepatic artery diameter could be predicted from the body weight (*BW*) by the following equation: $PHA = 0.07841+0.00147 \times BW$ for non-tumor-bearing rats, and by $PHA = 0.48045+0.00033 \times BW$, for tumor-bearing rats, with an overall model fit $R^2 = 0.30$. Second, the relationship between the diameter of the PHA artery and weight is not the same for SD and F344 rats (interaction = 0.00065472; *P* = 0.0002). Similar to the SD model, weight (coefficient = 0.00033058; *P* = 0.003), and rats' strain (coefficient = -0.27491; *P* < 0.0001) were significant predictors in the F344 rats. A positive interaction coefficient, in this case, indicates that the diameter of the PHA increases more rapidly with weight for the F344 than for SD rats. In this model, taking into account the rat strain, the PHA diameter could be predicted from animal's body weight (BW) by the following equation: $PHA = 0.20554+0.00099 \times BW$ for the F344, with an overall model fit of $R^2 = 0.51$. Although estimated in two separate analyses, the size of the PHA for tumor-bearing SD rats can be predicted using the same equation described above.

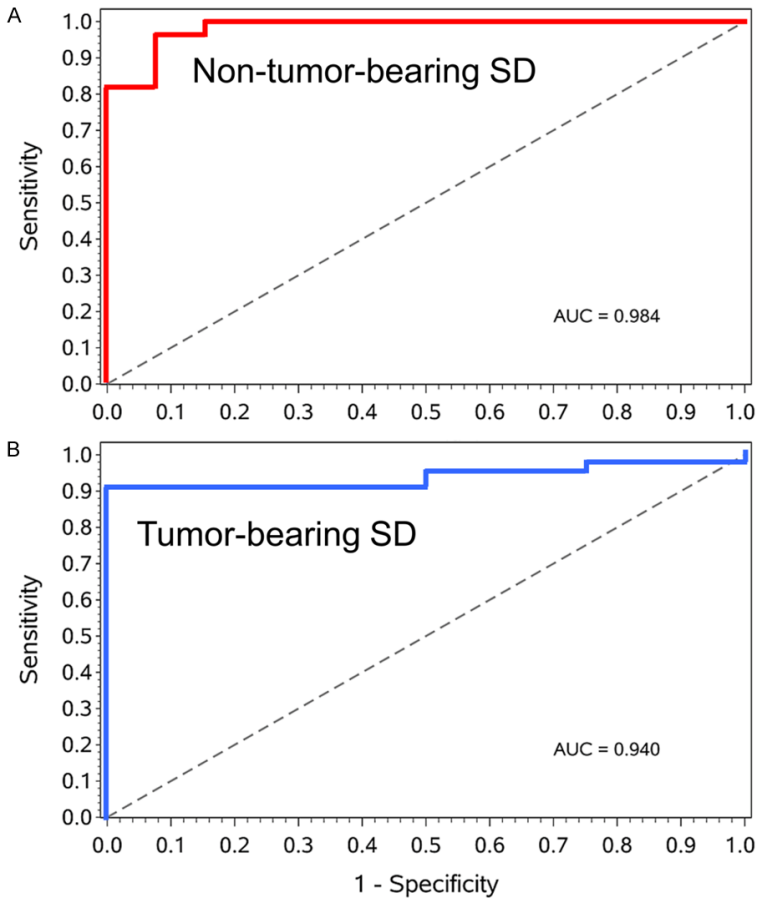

Figure 3. Receiver operating characteristic curves predicting the technical success of proper hepatic artery catheterization according to the animal's weight. A. Receiver operating characteristic curve of non-tumor-bearing Sprague-Dawley rats using a body weight cutoff ≤ 308 g, sensitivity, and specificity 96.4% and 92.3%. B. Receiver operating characteristic curve of tumor-bearing Sprague-Dawley rats using a body weight of cutoff ≥ 250 g; sensitivity and specificity of 91.3% and 100.0%. AUC: Area under the curve.

Technical success of transcatheter arterial embolization influenced by body weight

The overall technical success rate of proper hepatic catheterization for Sprague-Dawley rats was 81.32% (74/91). Hepatic artery catheterization was achieved in 92% (46/50) of the tumor-bearing rats and 68.3% (28/41) of the rats in the non-tumor group. **Table 2** summarizes results of the logistic regression model using the technical success of the procedure, defined as the stable placement of the microcatheter tip into the PHA, as the response and animals' weight as the predictor. The fit of the logistic regression model, assessed by the area under the receiver operating characteristic curve (AUC), yielded an AUC of 0.98, and a *P* value for the Hosmer-Lemeshow (HL) goodness-of-fit of 0.99 and R^2 = 0.86. The model predicts that by dichotomizing the body weight of non-tumor-bearing rats at 308 grams, technical success of the procedure could be anticipated, excluding those animals who died of surgical complications during the carotid artery cannulation. Therefore, for animals with body weight ≤ 308 grams the procedure is expected to fail due to a narrower PHA. Such a decision rule generates a sensitivity of 96.4% with 95% Clopper-Pearson confidence intervals of 81.65-99.91 and specificity of 92.3% [95% CI; 63.97-99.81] (**Figure 3A**). Similarly, logistic regression was fitted to the 50 tumor-bearing Sprague-Dawley rats, using the same parameters described above, yielding an AUC of 0.94 with an optimal cut-off value of 250 grams (**Figure 3B**). The HL goodness-of-fit for this model was 0.91 and R^2 = 0.48, therefore indicating that the model fits the data well. Moreover, the results of the model imply that for animals weighing ≥ 250 grams a stable placement of the microcatheter tip into the PHA is likely to be achieved. Such a decision rule generates a sensitivity and specificity of 91.3% [95% CI; 79.21-97.58] and 100.0% [95% CI; 39.79-100.00], respectively.

Discussion

Rodent models are increasingly playing a central role in interventional oncology research. Important drawbacks for implementation of catheter-based procedures in rats have been complexity of embolization procedure and limited survival after embolization. In this study, we described the main determinants of technical success in one of the most commonly used rat strains in IO and established a correlation between these determinants and fea-

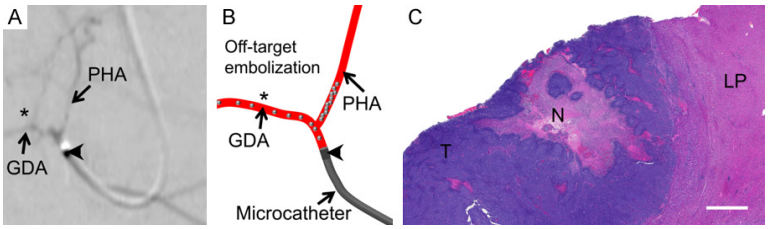

Figure 4. Relevance of animal's body weight at the time of hepatic artery catheterization. (A) Digital subtraction angiography depicting a suboptimal catheter position (arrowhead) due to a narrower artery diameter in a tumor-bearing Sprague-Dawley rat weighing less than 250 g at the time of catheterization. (B) Schematic representation showing a microcatheter positioned below the gastroduodenal artery (GDA) and proper hepatic artery (PHA). In this case, embolic material (i.e., drug-eluting beads, gelatin sponge, Intra-arterial chemotherapy) injected through a microcatheter larger than the nominal diameter of the PHA can increase the risk of off-target embolization (asterisk) or incomplete treatment of the HCC tumor nodules. (C) Histological micrograph of hematoxylin and eosin (H&E) stained tissue section of the same animal shown in (A), portraying incomplete embolization of the target lesion due to suboptimal catheter placement. Viable tumor (T), Normal liver parenchyma (NL) and tumor tissue necrosis (N). Scale bar: 1 mm.

sibility of arterial catheterization. Our results demonstrated that technical success of transcatheter arterial embolization using transcarotid approach is proportional to the animal's body weight at the time of catheterization. Our results also indicated that the right hepatic artery is consistently smaller than its left counterpart in these two rat strains and remains smaller irrespective of the presence of liver tumor. The relationship between the diameter of the PHA and the weight of the animals is significantly influenced by the presence of the tumor. Although this relationship is more pronounced for F344 rats than for the SD tumor-bearing rats, the weight-diameter association is preserved independently of the presence of the tumor, as observed in SD tumor-free rats.

Recent technical advances in arterial access and endovascular techniques have enabled investigators to consistently perform hepatic angiography and catheter-based interventions in orthotopic rat liver tumor models without the need for laparotomy, thus closely mimicking procedures performed in patients. Transcatheter arterial embolization of rat liver tumors is increasingly successful with studies using both transcarotid or transfemoral access as routes to the hepatic artery [15-18]. When compared to direct gastroduodenal cannulation, these approaches have the advantage of substantially reducing surgical trauma by eliminating additional abdominal surgeries [15, 20, 21] or GDA arteriotomy [22-28]. For rats undergoing these procedures, instances of technical failure are typically secondary to difficulty advancing the microcatheter into the diminutive diameter of hepatic vessels or substantial nontarget embolization [16, 18] (**Figure 4A**, **4B**). Changes in the diameter of the hepatic vasculature in relation to the overall liver weight have been previously reported in a correlative study between rodents and human livers, where authors have shown that liver perfusion increases along with the size of the liver [29]. Our results in regard to the proper hepatic diameter are also in agreement with a previous study published by Martins and Neuhaus, in which under direct observation using a surgical microscope, they have found proper hepatic artery diameters ranging from 0.2 to 0.5 millimeters in Wistar rats weighing 250-300 g [30], suggesting that diameters of hepatic vasculature are relatively conserved among different rats' strains. Furthermore, our findings confirm that this association is linear and enable investigators to accurately infer the size of hepatic arterial vasculature by simply measuring body weight. This knowledge can expedite animal screening and reduce unsuccessful procedures, as well as experimental costs. This relationship is explained by mechanisms of tumor vascularization in the liver [31], as the blood supply of hepatic tumors shifts from the portal vein to the hepatic artery [32].

Our results establish that investigators should avoid conducting studies in animals weighing ≤ 250 grams in case of tumor-bearing rats and ≤ 308 grams for non-tumor-bearing rats, given the increased risk of technical failure due to diminutive hepatic vessel size. By using the above-mentioned body weight cutoff points, we were able to confidently predict technical success, with sufficient sensitivity and specificity. We observed that the size of the RHA was smaller than the LHA in both rats' strains. The LHA remained constantly larger with or without the presence of liver tumor (s). Anatomic con-

siderations such as RHA or LHA vessel size and tortuosity should be taken into account for each individual rat strain before performing tumor inoculation into a specific liver lobe, when selective lobar catheterization is anticipated. Familiarity with these features is critical to minimize technical difficulties, when cannulating the proper hepatic artery or distal hepatic vasculature, thus reducing potential for vasospasm and non-target or incomplete embolization (**Figure 4B**, **4C**).

Seminal studies describing the hepatic vascular anatomy have reported key anatomical differences in the development of the hepatobiliary system between mice, rats, and humans [30, 33, 34]. It is important to highlight the fact that the absence of the gallbladder, cystic duct and cystic artery [33, 35] in rats, prevent the appearance of biliary complications, occasionally observed in clinical practice following TACE. It is also important to consider the presence of collateral vessels arising from GDA and the existence of the hepato-esophageal artery, branching from the proximal left hepatic artery [30, 36]. In spite of the fact that these secondary vessels are difficult to visualize during fluoroscopy-guided hepatic arterial catheterization, the embolization or incomplete embolization of such vessels respectively, can negatively impact treatment outcomes.

The present study has several limitations. First, we only included males in our experiments, therefore, additional correlative studies are needed to confirm if our observations apply to female rats. Second, we did not evaluate the procedural success in F344 rats, since the microcatheter (1.9-F) was bigger than the average diameter of the proper hepatic artery. Therefore, the optimal placement of the catheter into the hepatic artery was not always feasible. For this reason, the sample size used to determine the best body weight cutoff values to maximize the success rates was limited to ninety-one animals and only a single rat strain. Despite this substantial limitation, we chose to include the F344 data to illustrate that important anatomic and technical considerations are consistent among different strains.

In conclusion, this study demonstrates that the animal's body weight at the time of catheterization is the main determinant of technical success for transcatheter arterial embolization in orthotopic rat liver tumors. The association between body weight and hepatic artery diameter is linear, and investigators can objectively estimate the size of hepatic arterial vasculature. Familiarity with these technical considerations could expedite animal selection, improve technical success rates, as well as limit experimental costs.

Acknowledgements

This study was supported by Biocompatibles UK Ltd (BTG), Surrey, UK, Grant # BTG-SP-08.004-F01, and Sister Institution Network Fund (SINF) Grant # SINF-600801-80-115693-21.

Disclosure of conflict of interest

None.

Address correspondence to: Rony Avritscher, Department of Interventional Radiology, The University of Texas MD Anderson Cancer Center, 1515 Holcombe Blvd, Houston 77030, Texas, USA. Tel: 713-563-7913; Fax: 713-792-4098; E-mail: rony.avritscher@mdanderson.org

References

[1] Forner A, Reig M and Bruix J. Hepatocellular carcinoma. Lancet 2018; 391: 1301-1314.

[2] Kudo M, Finn RS, Qin S, Han KH, Ikeda K, Piscaglia F, Baron A, Park JW, Han G, Jassem J, Blanc JF, Vogel A, Komov D, Evans TRJ, Lopez C, Dutcus C, Guo M, Saito K, Kraljevic S, Tamai T, Ren M and Cheng AL. Lenvatinib versus sorafenib in first-line treatment of patients with unresectable hepatocellular carcinoma: a randomised phase 3 non-inferiority trial. Lancet 2018; 391: 1163-1173.

[3] El-Khoueiry AB, Sangro B, Yau T, Crocenzi TS, Kudo M, Hsu C, Kim TY, Choo SP, Trojan J, Welling TH Rd, Meyer T, Kang YK, Yeo W, Chopra A, Anderson J, Dela Cruz C, Lang L, Neely J, Tang H, Dastani HB, Melero I. Nivolumab in patients with advanced hepatocellular carcinoma (CheckMate 040): an open-label, non-comparative, phase 1/2 dose escalation and expansion trial. Lancet 2017; 389: 2492-2502.

[4] Palasca O, Santos A, Stolte C, Gorodkin J and Jensen LJ. TISSUES 2.0: an integrative web resource on mammalian tissue expression. Database (Oxford) 2018; 2018: 1-12.

[5] Shimoyama M, Smith JR, Bryda E, Kuramoto T, Saba L and Dwinell M. Rat genome and model resources. ILAR J 2017; 58: 42-58.

[6] De Minicis S, Kisseleva T, Francis H, Baroni GS, Benedetti A, Brenner D, Alvaro D, Alpini G and Marzioni M. Liver carcinogenesis: rodent models of hepatocarcinoma and cholangiocarcinoma. Dig Liver Dis 2013; 45: 450-459.
[7] Maataoui A, Qian J, Vossoughi D, Khan MF, Oppermann E, Bechstein WO and Vogl TJ. Transarterial chemoembolization alone and in combination with other therapies: a comparative study in an animal HCC model. Eur Radiol 2005; 15: 127-133.
[8] Sheu AY, Zhang Z, Omary RA and Larson AC. Invasive catheterization of the hepatic artery for preclinical investigation of liver-directed therapies in rodent models of liver cancer. Am J Transl Res 2013; 5: 269-278.
[9] Bastian P, Bartkowski R, Kohler H and Kissel T. Chemo-embolization of experimental liver metastases. Part I: distribution of biodegradable microspheres of different sizes in an animal model for the locoregional therapy. Eur J Pharm Biopharm 1998; 46: 243-254.
[10] Qian J, Vossoughi D, Woitaschek D, Oppermann E, Bechstein WO, Li WY, Feng GS and Vogl T. Combined transarterial chemoembolization and arterial administration of bletilla striata in treatment of liver tumor in rats. World J Gastroenterol 2003; 9: 2676-2680.
[11] Lee J, Gordon AC, Kim H, Park W, Cho S, Lee B, Larson AC, Rozhkova EA and Kim DH. Targeted multimodal nano-reporters for pre-procedural MRI and intra-operative image-guidance. Biomaterials 2016; 109: 69-77.
[12] Kim DH, Li W, Chen J, Zhang Z, Green RM, Huang S and Larson AC. Multimodal imaging of nanocomposite microspheres for transcatheter intra-arterial drug delivery to liver tumors. Sci Rep 2016; 6: 29653.
[13] Lindell B, Aronsen KF and Rothman U. Repeated arterial embolization of rat livers by degradable microspheres. Eur Surg Res 1977; 9: 347-356.
[14] Deng SG, Wu ZF, Li WY, Yang ZG, Chang G, Meng FZ and Mo LL. Safety of Curcuma aromatica oil gelatin microspheres administered via hepatic artery. World J Gastroenterol 2004; 10: 2637-2642.
[15] Li X, Wang YX, Zhou X, Guan Y and Tang C. Catheterization of the hepatic artery via the left common carotid artery in rats. Cardiovasc Intervent Radiol 2006; 29: 1073-1076.
[16] Kiefer RM, Hunt SJ, Pulido S, Pickup S, Furth EE, Soulen MC, Nadolski GJ and Gade TP. Relative initial weight is associated with improved survival without altering tumor latency in a translational rat model of diethylnitrosamine-induced hepatocellular carcinoma and transarterial embolization. J Vasc Interv Radiol 2017; 28: 1043-1050, e2.
[17] Ju S, McLennan G, Bennett SL, Liang Y, Bonnac L, Pankiewicz KW and Jayaram HN. Technical aspects of imaging and transfemoral arterial treatment of N1-S1 tumors in rats: an appropriate model to test the biology and therapeutic response to transarterial treatments of liver cancers. J Vasc Interv Radiol 2009; 20: 410-414.
[18] Gade TP, Hunt SJ, Harrison N, Nadolski GJ, Weber C, Pickup S, Furth EE, Schnall MD, Soulen MC and Celeste Simon M. Segmental transarterial embolization in a translational rat model of hepatocellular carcinoma. J Vasc Interv Radiol 2015; 26: 1229-1237.
[19] Schindelin J, Arganda-Carreras I, Frise E, Kaynig V, Longair M, Pietzsch T, Preibisch S, Rueden C, Saalfeld S, Schmid B, Tinevez JY, White DJ, Hartenstein V, Eliceiri K, Tomancak P and Cardona A. Fiji: an open-source platform for biological-image analysis. Nat Methods 2012; 9: 676-682.
[20] Desborough JP. The stress response to trauma and surgery. Br J Anaesth 2000; 85: 109-117.
[21] Davenport L, Letson HL and Dobson GP. Immune-inflammatory activation after a single laparotomy in a rat model: effect of adenosine, lidocaine and Mg(2+) infusion to dampen the stress response. Innate Immun 2017; 23: 482-494.
[22] Fang ZT, Wang GZ, Zhang W, Qu XD, Liu R, Qian S, Zhu L, Zhou B and Wang JH. Transcatheter arterial embolization promotes liver tumor metastasis by increasing the population of circulating tumor cells. Onco Targets Ther 2013; 6: 1563-1572.
[23] Wang GZ, Fang ZT, Zhang W, Qu XD, Qian S, Liu R and Wang JH. Increased metastatic potential of residual carcinoma after transarterial embolization in rat with McA-RH7777 hepatoma. Oncol Rep 2014; 31: 95-102.
[24] Ni JY, Xu LF, Wang WD, Huang QS, Sun HI and Chen YT. Transarterial embolization combined with RNA interference targeting hypoxia-inducible factor-1α for hepatocellular carcinoma: a preliminary study of rat model. J Cancer Res Clin Oncol 2017; 143: 199-207.
[25] Chen C, Wang J, Liu R and Qian S. RNA interference of hypoxia-inducible factor-1 alpha improves the effects of transcatheter arterial embolization in rat liver tumors. Tumour Biol 2012; 33: 1095-1103.
[26] Chen CS, Zhao Q, Qian S, Li HL, Guo CY, Zhang W, Yan ZP, Liu R and Wang JH. Ultrasound-guided RNA interference targeting HIF-1 alpha improves the effects of transarterial chemoembolization in rat liver tumors. Onco Targets Ther 2015; 8: 3539-3548.
[27] Wang BM and Li N. Effect of the Wnt/beta-catenin signaling pathway on apoptosis, migra-

tion, and invasion of transplanted hepatocellular carcinoma cells after transcatheter arterial chemoembolization in rats. J Cell Biochem 2018; 119: 4050-4060.
[28] Vogl TJ, Oppermann E, Qian J, Imlau U, Tran A, Hamidavi Y, Korkusuz H, Bechstein WO, Nour-Eldin NE, Gruber-Rouh T, Hammerstingl R and Naguib NN. Transarterial chemoembolization of hepatocellular carcinoma in a rat model: the effect of additional injection of survivin siRNA to the treatment protocol. BMC Cancer 2016; 16: 325-333.
[29] Kruepunga N, Hakvoort TBM, Hikspoors JPJM, Köhler SE and Lamers WH. Anatomy of rodent and human livers: what are the differences? Biochim Biophys Acta Mol Basis Dis 2019; 1865: 869-878.
[30] Martins PN and Neuhaus P. Surgical anatomy of the liver, hepatic vasculature and bile ducts in the rat. Liver Int 2007; 27: 384-392.
[31] Dezso K, Bugyik E, Papp V, Laszlo V, Dome B, Tovari J, Timar J, Nagy P and Paku S. Development of arterial blood supply in experimental liver metastases. Am J Pathol 2009; 175: 835-843.
[32] Chen L, Zheng Y, Zhang H, Pan H, Liu Q, Zhou X, Wei W, Liu Y, Zhen M, Wang J, Zhou J and Zhao Y. Comparative analysis of tumor-associated vascular changes following TACE alone or in combination with sorafenib treatment in HCC: a retrospective study. Oncol Lett 2018; 16: 3690-3698.
[33] Vdoviaková K, Vdoviaková K, Petrovová E, Krešáková L, Maloveská M, Teleky J, Jenčová J, Živčák J and Jenča A Jr. Importance rat liver morphology and vasculature in surgical research. Med Sci Monit 2016; 22: 4716-4728.
[34] Madrahimov N, Dirsch O, Broelsch C and Dahmen U. Marginal hepatectomy in the rat: from anatomy to surgery. Ann Surg 2006; 244: 89-98.
[35] Higashiyama H, Uemura M, Igarashi H, Kurohmaru M, Kanai-Azuma M and Kanai Y. Anatomy and development of the extrahepatic biliary system in mouse and rat: a perspective on the evolutionary loss of the gallbladder. J Anat 2018; 232: 134-145.
[36] Leneman F and Burton S. The hepato-esophageal artery of the rat. Brief report. Acta Anat (Basel) 1967; 68: 334-343.